Single molecule magnetic behaviour in lanthanide naphthalenesulfonate complexes

Article (Accepted Version)

Journal Name

ARTICLE

Single molecule magnetic behaviour in lanthanide naphthalenesulfonate complexes

Received 00th January 20xx,
Accepted 00th January 20xx

DOI: 10.1039/x0xx00000x

www.rsc.org/

Guo Peng,*[a] Ying-Ying Zhang,[a] Bo Li,*[b] Xiao-Fan Sun,[c] Hong-Ling Cai,[c] De-Jing Li,[d] Zhi-Gang Gu[d] and George E. Kostakis [e]

The use of 2-naphthalenesulfonate (NAS) ligand in lanthanide chemistry afforded a family of isostructural mononuclear lanthanide complexes with formula $[Ln(NAS)_2(H_2O)_6](NAS)\cdot 3H_2O$ [Ln = Tb (**1**), Dy (**2**), Er (**3**), Yb (**4**)]. Crystallographic studies determine a square antiprismatic geometry (D_{4d}) for the Ln centre and crystallization in unprecedented chiral space group. The latter was further confirmed by the observation of Cotton effects in single crystal circular dichroism (CD) spectra. Static and dynamic magnetic measurements identify weak intermolecular dipolar interactions in **2**, and such effects can be waived by dilution, which was noted by the detection of zero-field single molecule magnet (SMM) behaviour and hysteresis loop in the magnetically diluted sample (**5**). Compounds **2-4** exhibit SMM behaviours with energy barriers of 53, 32 and 45 K, respectively. To the best of our knowledge, these complexes provide the first examples of pure 4f sulfonate-based SMMs.

Introduction

The intriguing features of compounds behaving as single molecule magnets (SMMs) such as slow relaxation of magnetization and hysteresis loop, ultra-small and uniform sizes, and detectable quantum tunnelling of magnetization (QTM) [1] are valuable parameters for the development of high-density data storage, molecular spintronics and quantum computing technologies.[2] The dynamic magnetization of the SMMs is governed by the magnetic anisotropy of the metal centres and therefore lanthanides (Ln) which have significant single ion magnetic anisotropy, because of the strong spin-orbital coupling are excellent candidates for the synthesis of SMMs.[3]

More specifically, it is well documented that the magnetic anisotropy of Ln is strongly related with the ligand field and local coordination geometry.[4] Prominent ligand field with highly symmetric coordination environment can maximize the axial anisotropy and thus suppress the quantum tunnelling of magnetization (QTM), leading to high energy barriers and / or blocking temperatures. This has been proved by the excellent performance of Ln SMMs with pseudo-C_∞, D_{5h} or D_{4d} symmetry.[5-8] Therefore, it becomes evident that the selection of the appropriate organic ligand to waive the orbital degeneracy as well as maintain the high coordination symmetry for the Ln ions is a crucial aspect in the synthesis of Ln based SMMs. To this direction, a variety of organic ligands with limited or several coordination sites such as Schiff base,[9] diketone,[10] phthalocyaninate and its derivatives,[8, 11] carboxylate,[12] phosphonate / phosphine oxides,[6, 13] alcohols / phenols,[7, 14] cyclopentadienide / cyclooctatetraenide[5, 15] and ethanolamine[16] have been used to build coordination entities with SMM behaviour.

Phosphonate ($R\text{-}PO_3$) ligands have been employed for the synthesis of Ln SMMs,[13] however the corresponding sulfonate ($R\text{-}SO_3$) ligands have been less used in the synthesis of Ln complexes,[17] and consequently for the synthesis of Ln-based SMMs. To the best of our knowledge, no systematic investigation for the dynamic magnetic properties of sulfonate-based lanthanide complexes has been explored, although some 3d or 3d-4f coordination compounds showing SMM behaviours have been documented before.[18] Having all these in mind, we initiated a project to study the coordination properties of sulfonate based ligands with Ln ions as well as study the magnetic properties of the resulting compounds. We considered the 2-naphthalenesulfonate organic ligand as the starting point of our investigation, therefore we report herein a family of mononuclear lanthanide complexes formulated as $[Ln(NAS)_2(H_2O)_6](NAS)\cdot 3H_2O$ [Ln = Tb (**1**), Dy (**2**), Er (**3**), Yb (**4**); NSA = 2-naphthalenesulfonate] and

[a] Herbert Gleiter Institute of Nanoscience, School of Materials Science and Engineering, Nanjing University of Science and Technology, 210094 Nanjing, P. R. China. Email: guopeng@njust.edu.cn
[b] College of Chemistry and Pharmaceutical Engineering, Nanyang Normal University, Nanyang 473061, P. R. China. Email: libozzu0107@163.com
[c] Collaborative Innovation Center of Advanced Microstructures, Lab of Solid State Microstructures, School of Physics, Nanjing University, Nanjing 210093, P. R. China.
[d] State Key Laboratory of Structural Chemistry, Fujian Institute of Research on the Structure of Matter, Chinese Academy of Sciences, 350002 Fuzhou, P. R. China.
[e] Department of Chemistry, School of Life Sciences, University of Sussex, Brighton, BN1 9QJ, UK.

Electronic Supplementary Information (ESI) available: IR spectra, PXRD patterns, TGA and DSC curves, additional magnetic data, tables, dielectric and ferroelectric plots. CCDC 1862026 for **1**. See DOI: 10.1039/x0xx00000x

$[Dy_{0.06}Y_{0.94}(NAS)_2(H_2O)_6](NAS)\cdot 3H_2O$ (**5**). Some of these compounds have been reported before,[17a, b] but their magnetic behaviour has not been studied. Moreover, our choice to isolate the Tb analogue (**1**) and the magnetically diluted sample $Dy_{0.06}Y_{0.94}$ (**5**) was crucial to elucidate the dynamic magnetic properties of these compounds. Furthermore, circular dichroism, TGA and DSC, dielectric and ferroelectric studies are also discussed.

Experimental section

General Materials and Methods

All the chemicals used in the reactions were commercially available and were used as received without further purification. Compounds **1**-**4** were prepared by modifying a reported procedure.[17a, b] Elemental analyses (C, H, and S) were conducted on a Vario MICRO cube elemental analyzer. Fourier transform infrared (IR) spectra were recorded on a Nicolet IS10 Spectrum with samples in the form of KBr discs. The circular dichroism (CD) spectra were obtained from solid-state samples in KBr pellets using a Bio-logic MOS-450 CD Spectrometer. The inductively coupled plasma (ICP) atomic emission spectrum was recorded on a Rayleigh AS-20 spectrometry. Powder X-Ray diffraction (PXRD) patterns for all compounds were measured at room temperature by a Bruker D8 ADVANCE X-ray diffractometer. Thermal gravimetric analyses (TGA) were carried out on a Mettler-Toledo TGA/SDTA851 thermoanalyzer using a heating rate of 10 K / min at nitrogen atmosphere. Differential scanning calorimetry (DSC) tests were conducted on a Mettler-Toledo DSC 1 instrument using a heating rate of 5 K / min at nitrogen atmosphere. Direct current (dc) magnetic measurements for all complexes were carried out on a Quantum Design PPMS DynaCool-9 magnetometer. The magnetic data were corrected for diamagnetic contribution by using Pascal's constants. Altering current (ac) magnetic measurements for **1** were performed on a Quantum Design MPMS-XL SQUID magnetometer, while such measurements for **2**-**4** were conducted on a Quantum Design MPMS3 SQUID magnetometer. Dielectric permittivities were tested on a Tonghui TH2828A LCR meter. The P-E hysteresis loops measurements were documented using a Precision Premier II Ferroelectric Tester.

Synthesis of $[Tb(NAS)_2(H_2O)_6](NAS)\cdot 3H_2O$ (1). Sodium 2-naphthalenesulfonate (0.691 g, 3 mmol) and $TbCl_3\cdot 6H_2O$ (0.373 g, 1 mmol) were dissolved in a mixture of C_2H_5OH (14 mL) and H_2O (7 mL). The resulting mixture was heated at 55ºC for 3h and then filtered when the solution was cooled. Slow evaporation of the filtrate at room temperature gave colourless crystals after several days. The crystals were separated by filtration, washed with C_2H_5OH, and dried in the air. Yield: 428 mg (45 % based on Tb). Calc. (%) for $C_{30}H_{39}TbO_{18}S_3\cdot 0.2C_2H_5OH$: C 38.36, H 4.26; S 10.11; found: C 38.60, H 3.98, S 10.32. Selected IR data (cm^{-1}): 3443 (br), 1648 (w), 1504 (w), 1349 (w), 1168 (s), 1096 (s), 1038 (s), 898 (w), 817 (m), 750 (w), 676 (m), 626 (w), 559 (w), 476 (w) (Fig. S1).

Synthesis of $[Dy(NAS)_2(H_2O)_6](NAS)\cdot 3H_2O$ (2). Complex **2** was synthesized via the procedure similar with **1** except that the $TbCl_3\cdot 6H_2O$ was replaced by $DyCl_3\cdot 6H_2O$ (0.378 g, 1 mmol). Yield: 308 mg (32 % based on Dy). Calc. (%) for $C_{30}H_{39}DyO_{18}S_3\cdot 0.2C_2H_5OH$: C 38.21, H 4.24; S 10.07; found: C 38.49, H 4.14, S 10.29. Selected IR data (cm^{-1}): 3446 (br), 1648 (w), 1504 (w), 1348 (w), 1169 (s), 1096 (s), 1038 (s), 898 (w), 817 (m), 750 (w), 676 (m), 626 (w), 559 (w), 476 (w) (Fig. S1).

Synthesis of $[Er(NAS)_2(H_2O)_6](NAS)\cdot 3H_2O$ (3). Complex **3** was synthesized via the procedure similar with **1** except that the $TbCl_3\cdot 6H_2O$ was replaced by $ErCl_3\cdot 6H_2O$ (0.382 g, 1 mmol). Yield: 516 mg (54 % based on Er). Calc. (%) for $C_{30}H_{39}ErO_{18}S_3\cdot 0.2C_2H_5OH$: C 38.02, H 4.22; S 10.02; found: C 38.25, H 4.04, S 10.27. Selected IR data (cm^{-1}): 3452 (br), 1648 (w), 1504 (w), 1348 (w), 1169 (s), 1096 (s), 1039 (s), 898 (w), 817 (m), 751 (w), 676 (m), 626 (w), 560 (w), 476 (w) (Fig. S1).

Synthesis of $[Yb(NAS)_2(H_2O)_6](NAS)\cdot 3H_2O$ (4) Complex **4** was synthesized via the procedure similar with **1** except that the $TbCl_3\cdot 6H_2O$ was replaced by $YbCl_3\cdot 6H_2O$ (0.388 g, 1 mmol). Yield: 537 mg (56 % based on Yb). Calc. (%) for $C_{30}H_{39}YbO_{18}S_3\cdot 0.1C_2H_5OH$: C 37.73, H 4.15; S 10.01; found: C 37.95, H 4.04, S 10.25. Selected IR data (cm^{-1}): 3451 (br), 1648 (w), 1504 (w), 1348 (w), 1169 (s), 1096 (s), 1039 (s), 898 (w), 817 (m), 751 (w), 675 (m), 626 (w), 559 (w), 476 (w) (Fig. S1).

Synthesis of $[Dy_{0.06}Y_{0.94}(NAS)_2(H_2O)_6](NAS)\cdot 3H_2O$ (5). The magnetically diluted sample was synthesized via the procedure similar with **1** except that the $TbCl_3\cdot 6H_2O$ was replaced by a mixture of $DyCl_3\cdot 6H_2O$ (0.019 g, 0.05 mmol) and $YCl_3\cdot 6H_2O$ (0.288 g, 0.95 mmol) in molar ratios of 1 : 19. The Dy content in the final product is ~6% determined by ICP technique. Yield: 400 mg (43 % based on Y). Calc. (%) for $C_{30}H_{39}Dy_{0.06}Y_{0.94}O_{18}S_3\cdot 0.1C_2H_5OH$: C 41.14, H 4.53; S 10.91; found: C 41.43, H 4.36, S 11.24. Selected IR data (cm^{-1}): 3447 (br), 1648 (w), 1504 (w), 1348 (w), 1169 (s), 1096 (s), 1039 (s), 898 (w), 817 (m), 750 (w), 676 (m), 626 (w), 560 (w), 476 (w) (Fig. S1).

Crystal structure determination and refinement

The crystallographic data of **1**-**4** were collected on a Bruker SMART APEX II diffractometer using monochromated Mo-Kα radiation (λ = 0.71073 Å) at 173(2) K. The sorption corrections were performed using TWINABS for **3** and SADABS for **1**, **2** and **4** supplied by Bruker. All structures were solved by direct methods and refined by full-matrix least squares analysis on F^2, using the SHELXTL program package[19]. The crystal of **3** is a non-merohedral twin, while the crystals of **1, 2** and **4** are two-component inversion twin. Ordered non-H atoms were refined anisotropically, H-atoms were placed in calculated positions and refined using a riding model. In order to check if there are phase transitions below room temperature, the crystallographic data of **2** were also recorded at 296(2) K. The data collected at 296(2) K can also be refined well in $P2_1$ space group (**2a**), indicating no phase transitions occurs below room temperature. Details of the crystal structures, data collection and refinement are summarized in Table 1.

Results and discussions

Synthesis and structure

The reactions of NAS and $LnCl_3 \cdot 6H_2O$ (Ln = Tb, Dy, Er, Yb) salts in a molar ratio 3 : 1 in the mixed solvent system (C_2H_5OH / H_2O = 2 : 1) yields compounds **1**-**4**. The use of other Ln salts such as $Ln(OTf)_3$ or $Ln(NO_3)_3 \cdot 6H_2O$ in place of $LnCl_3 \cdot 6H_2O$, affords the same product, but in lower yield. The use of perchlorate or diketonate Ln salts such as $Ln(ClO_4)_3 \cdot 6H_2O$ or $Ln(acac)_3$ in place of $LnCl_3 \cdot 6H_2O$, under similar reaction conditions does not yield a crystalline material. Compounds **1** and **2** can also be prepared by employing 2-naphthalenesulfonic acid as starting material, however this methodology is not efficient for the synthesis of compounds **3** and **4**.

Table 1 Crystallographic data and structure refinement for complexes **1**-**4**.

	1	2#	2a#	3#	4#
Formula	$C_{30}H_{39}O_{18}S_3Tb$	$C_{30}H_{39}DyO_{18}S_3$	$C_{30}H_{39}DyO_{18}S_3$	$C_{30}H_{39}ErO_{18}S_3$	$C_{30}H_{39}O_{18}S_3Yb$
M_r (g mol^{-1})	942.71	946.29	946.29	951.05	956.83
Crystal system	Monoclinic	Monoclinic	Monoclinic	Monoclinic	Monoclinic
Space group	$P2_1$	$P2_1$	$P2_1$	$P2_1$	$P2_1$
T (K)	173(2)	173(2)	296(2)	173(2)	173(2)
a (Å)	14.0436(6)	14.0526(7)	14.0617(5)	13.9853(15)	13.9719(7)
b (Å)	7.4260(3)	7.4236(3)	7.4631(3)	7.4049(7)	7.3944(3)
c (Å)	18.0722(8)	18.0933(10)	18.1509(7)	18.032(2)	17.9881(8)
α (º)	90	90	90	90	90
β (º)	107.725(2)	107.732(2)	107.8200(10)	107.735(4)	107.7170(10)
γ (º)	90	90	90	90	90
V (Å^3)	1795.24(13)	1797.84(15)	1813.44(12)	1778.7(3)	1770.28(14)
Z	2	2	2	2	2
D_c (g cm^{-3})	1.744	1.748	1.733	1.776	1.795
μ (mm^{-1})	2.223	2.331	2.311	2.614	2.898
F(000)	952	954	954	958	962
Reflns collected	15343	9653	23259	-	27405
Unique reflns	6171	6314	7351	3353	7194
R_{int}	0.0617	0.0357	0.0549	-	0.0686
GOF	1.042	1.132	1.079	1.153	1.053
R_1(I > 2σ)	0.0325	0.0400	0.0331	0.0444	0.0411
wR_2 (all data)	0.0521	0.0789	0.0666	0.0815	0.0638
Max. diff. peak / hole (e Å^{-3})	0.417/-0.575	0.746/-1.077	0.630/-0.768	0.800/ -1.17	0.676/ -0.880
Flack parameter	0.239(10)	0.118(15)	-0.024(6)	0.130(17)	0.395(10)

#The structures of **2**-**4** have been reported before, [17a, b] therefore only the CCDC number of **1** is provided herein.

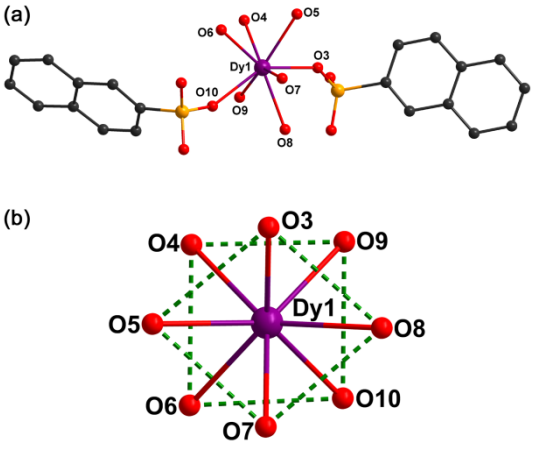

Fig. 1 Molecular structure of $[Dy(NAS)_2(H_2O)_6]^+$ cation (a) and the square antiprism coordination geometry of Dy(III) centre (b). Dy, O, S and C are shown in violet, red, yellow and black, respectively. H atoms and lattice anions are omitted for clarity.

Single crystal diffraction analyses show that all compounds reported in this work are isostructural to the previously reported derivatives[17a, b] and thus a brief description of the structure of **2** is given. Complex **2** crystallizes in the chiral space group $P2_1$ with Z = 2. There are one $[Dy(NAS)_2(H_2O)_6]^+$ cation, one NAS^- counterion and three lattice water molecules in the asymmetric unit (Fig. 1). The Dy(III) is eight coordinated with two oxygen donors from two NAS ligands and six oxygen atoms from six water molecules. The Dy-O distances are found in the 2.313(7)-2.388(6) Å range. The analysis based on continues shape measures (CShM) software [20] indicates that the coordination geometry around Dy(III) can be described as distorted square antiprism (D_{4d} symmetry) (Table S1). One square is constructed by the atoms O3, O5, O7 and O8, while the other is defined by the donors of O4, O6, O10 and O9 (Fig. 1b). The nearest intermolecular Dy(III)···Dy(III) separation is 7.4326(7) Å.

Circular dichroism spectra

Given the fact that compound **2** crystallizes in a chiral space group, the single crystal solid-state circular dichroism (CD) spectra of randomly selected crystals was recorded at room temperature (10 measurements in total). The CD spectra exhibit opposite Cotton effects at 230 and 299 nm (Fig. 2), suggesting the formation of enantiomers during the process of spontaneous resolution. The

nearly mirror imaged CD spectra of **2** confirms the optical active and enantiomeric nature of its crystals. The CD spectrum of the bulk

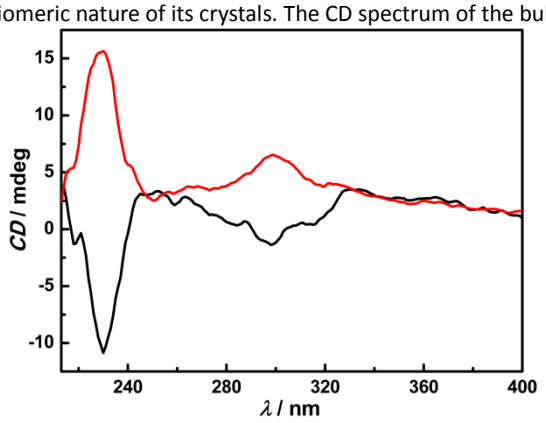

Fig. 2 Solid-state CD spectra of **2** at room temperature.

sample confirms that the resulting crystals are racemic mixture (Fig. S2).

PXRD, TGA and DSC studies

PXRD were carried out for all complexes to examine the purity of the bulk samples. The experimental PXRD patterns are consistent with that from simulation based on crystallographic data (Fig. S3), verifying the pure phase of as-synthesized products. The experimental PXRD patterns of complexes **1**-**5** suggest the isomorphous nature of these structures, which is in very good agreement with the results from single-crystal structure determination. To study the thermal stability of these complexes, TGA of **2** was conducted from 323 to 1073 K at a heating rate of 10 K / min at nitrogen atmosphere. Complex **2** remain stable until 353 K and start to decompose thereafter (Fig. S4). DSC measurements of **2** reveal that no structural phase transitions were detected from 123-353 K (Fig. S5). This phenomenon indicates that these complexes maintain the chiral structures below room temperature, which is consistent with the result of the single-crystal X-ray analysis.

Magnetic properties

The static magnetic properties of **1**-**4** were studied under 1000 Oe applied field in the temperature range of 2-300 K. Selected magnetic data obtained from these measurements are listed in Table S2. The room temperature χT products of all complexes are closed to the theoretic values for one separated Ln(III) ion. With the reduction of temperature, the χT products of **1**, **3** and **4** decrease continually until 2 K (Fig. 3), which is largely due to the thermal depopulation of the excited m_J sublevels of Ln(III) ions. For **2**, the χT product steadily decreases with cooling to a minimum of 10.71 cm^3 K mol^{-1} at 7.5 K and then abruptly increases to 11.30 cm^3 K mol^{-1} at 2 K (Fig. 3). This behaviour indicates that the presence of weak intermolecular dipolar interactions between different Dy(III) centres below 7.5 K, and the decrease above 7.5K is probably attribute to thermal depopulation of the excited m_J sublevels of Dy(III) ion. Isothermal magnetization curves of **1**-**4** increase smoothly with increasing applied magnetic field and reach 4.65, 5.09, 5.37 and 1.64 Nβ at 7 T and 2 K, respectively, which are far from saturation (Fig. S6). The lack of saturation and the observation of non-superposed M versus HT^{-1} curves (Fig. S7) suggest that the presence of anisotropy and / or low-lying excited states in these complexes.

In light of the existence of magnetic anisotropy, ac susceptibility measurements were performed to explore the dynamic magnetic properties. For **1** with non-Kramers ion of Tb(III), no clear out-of-phase ac signals were observed even under an applied field of up to 3000 Oe (Fig. S8). In the absence of dc field, clear out-of-phase ac components were detected below 6 K for **2** (Fig. 4a), suggesting slow relaxation of magnetization which is related to SMM behaviour. However, no well-defined maxima appear down to 2 K (Fig. 4a), which is probably ascribe to the fast quantum tunnelling of magnetization (QTM) promoting by intermolecular dipolar interactions. Such effect has also been observed in dc magnetic measurements. In order slow down the relaxation, further ac magnetic measurements were conducted for **2** at 4 K under

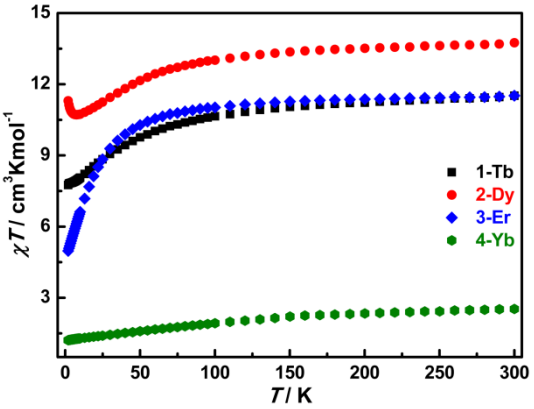

Fig. 3 Temperature dependence of the χT products of complexes **1**-**4**.

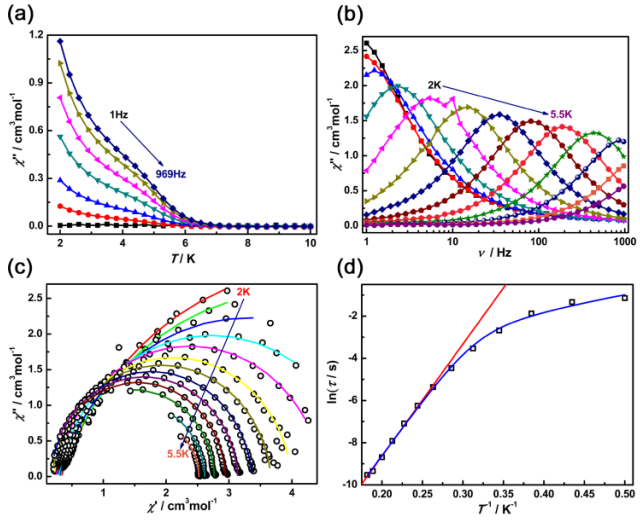

Fig. 4 Temperature (a) and frequency (b) dependence of out-of-phase ac susceptibility data under 0 (a) and 1000 Oe (b) dc fields for **2**. Cole-Cole plots for **2** (c). The solid lines are the best fits to a generalized Debye model. Temperature dependence of the relaxation times under 1000 Oe dc field for **2** (d). The red line is the

best fits to an Arrhenius law. The blue line is fit for Orbach plus Raman processes.

indicated dc fields. Clear peaks were detected in out-of-phase ac signals by the application of dc fields from 200 Oe to 2500 Oe (Fig. S9), indicating the suppression of QTM. Thus, a dc field of 1000 Oe was selected to further study the dynamic magnetization. This leads to strong out-of-phase ac signals with well-defined maxima (Fig. 4b), suggesting field-induced SMM behaviour of **2**. From the frequency dependent ac data at various temperatures, the Cole-Cole plots were constructed and fitted by a generalized Debye model (Fig. 4c).[21] This results in α = 0.0093-0.22 (Table S3), indicating narrow distribution of relaxation time. The relaxation times extracted from Cole-Cole plots fitting obey Arrhenius law above 3.8 K with an effective energy barrier of 53 K (τ_0 = 4.3×10^{-9} s) (Fig. 4d). The deviation of the relaxation times from linearity below 3.8 K suggests the presence of other relaxation process. Therefore, a model with Orbach and Raman processes was taken into account for the fitting (eqn. 1). The best fit gave an energy barrier of 52 K with C = 0.21 s^{-1} K$^{-3.7}$, n = 3.7, τ_0 = 5.1×10^{-9} s (Fig. 4d), which is in agreement with the results from linear Arrhenius fitting. For Raman process, the theoretic value for n is 9, but n = 1-6 is also reasonable when optical and acoustic phonons are considered. [22]

$$\tau^{-1} = \tau_0^{-1}\exp(-U_{eff}/k_BT) + CT^n \quad (1)$$

In order to minimized the effect of intermolecular dipolar interactions on the spin dynamics of Dy(III) ion, the magnetically diluted sample Dy@Y (**5**) was prepared. The out-of-phase ac signals of **5** display temperature and frequency dependent with clear maxima under a zero dc field (Fig. 5a, b), indicating a typical SMM behaviour, which is quite different from that of **1**. The appearance of peaks in the absence of dc field confirms that the magnetic relaxation was slowed down by dilution. However, the out-of-phase components after the maxima go up continually until 2 K (Fig. 5a) suggests that this system is still affected by QTM. It means that the QTM was only partly suppressed by dilution. Therefore, the dynamic magnetic properties of **5** were further studied by the application of 1000 Oe dc field (Fig. S10). In comparison with the data obtained from a zero dc field, the characteristic peaks under 1000 Oe dc field (Fig. 5c) move to low frequency region, indicating the QTM was efficiently suppressed. The Cole-Cole plots extracted from 0 and 1000 Oe dc field data can be fitted well by a generalized Debye model (Fig. S11), leading to α = 0.073-0.54 (Table S4) and α near to 0 (Table S5). The large α values under zero dc field indicates the presence of multiple relaxation processes, whereas the near zero α values under 1000 Oe dc field suggest that the narrow distribution of relaxation time. Linear fits to the relaxation times result in effective energy barriers of 54 K (τ_0 = 1.7×10^{-9} s) under zero dc field and 61 K (τ_0 = 1.1×10^{-9} s) under 1000 Oe dc field (Fig. 5d). In order to reproduce the temperature dependence of the relaxation times under zero dc field over the whole temperature range, Orbach, Raman, direct and τ_{QTM} relaxation processes were considered for the fitting, which is expressed as (eqn. 2):

$$\tau^{-1} = \tau_0^{-1}\exp(-U_{eff}/k_BT) + CT^n + AT + \tau_{QTM}^{-1} \quad (2)$$

However, no best fit can be obtained by including all these relaxation processes even fixed the U_{eff} and τ_0 deduced from linear Arrhenius fitting. To avoid over-parametrization, the fitting

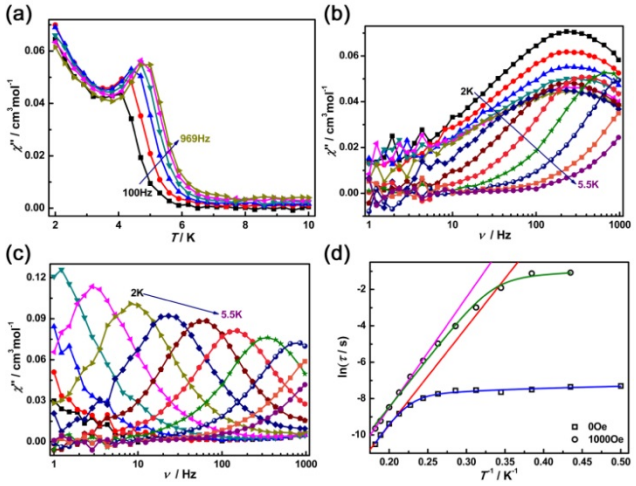

Fig. 5 Temperature (a) and frequency (b, c) dependence of out-of-phase ac susceptibility data under 0 (a, b) and 1000 Oe (c) dc fields for **5**. Temperature dependence of the relaxation times under 0 and 1000 Oe dc field for **5** (d). The red and pink lines are the best fits to an Arrhenius law. The blue line is fit for the sum of Orbach, direct and QTM processes. The green line is fit for Orbach plus direct processes.

procedure was addressed by considering the contribution of each process step by step, searching for the best fit using minimum number of fitting terms. Finally, the plots can be reproduced well by taking the Orbach, direct and τ_{QTM} processes into account (Fig. 5d), which yields the parameters τ_{QTM}^{-1} = 789 s^{-1}, A = 364 s^{-1} K^{-1} and U_{eff} = 65 K with τ_0 = 2.4×10^{-10} s. The QTM was quenched by the application of a 1000 Oe dc field. Therefore, only Orbach and direct processes were included for the fitting of τ versus T plot under 1000Oe dc field. This gives the parameters A = 1.3 s^{-1} K^{-1} and U_{eff} = 54 K with τ_0 = 4.8×10^{-9} s (Fig. 5d).

In the case of **3** and **4** with Kramers ions of Er(III) and Yb(III), no ac signals were observed under zero dc field above 2 K. However, the out-of-phase components of both complexes were switched on by the application of different dc field (Fig. S12 and S13). Thus, the frequency dependence ac susceptibility of these two complexes was further probed under 1000 Oe dc field. This results in strong out-of-phase ac signals with clear peaks (Fig. 6a, b), indicating both complexes are field-induced SMMs. The Cole-Cole plots of these two complexes can be fitted well (Fig. S14) by a generalized Debye model with α = 0-0.11 for **3** (Table S6) and 0-0.32 for **4** (Table S7), which suggests a narrow distribution of the relaxation time. The fit of the linear parts of relaxation times gave effective energy barriers of 32 K (τ_0 = 5.8×10^{-9} s) for **3** and 45 K (τ_0 = 5.1×10^{-8} s) for **4** (Fig. 6c). The Lnτ versus T^{-1} curves of **3** and **4** deviate from linearity at low temperature. Therefore, several models including different relaxation processes was tried to fit the relaxation times in the whole temperature range. For **3**, the best fit was obtained by taking Orbach and QTM processes into account (eqn. 3), producing parameters τ_{QTM}^{-1} = 198 s^{-1} and U_{eff} = 35 K with τ_0 = 2.4×10^{-9} s (Fig. 6c). In the case of **4**, Lnτ versus T^{-1} curve can be fitted well by

considering both Raman and QTM processes (eqn. 4), providing parameters $C = 6.8\times10^{-4}$ K$^{-9.3}$, $n = 9.3$, $\tau_{QTM}^{-1} = 2.6$ s^{-1} (Fig. 6c), which

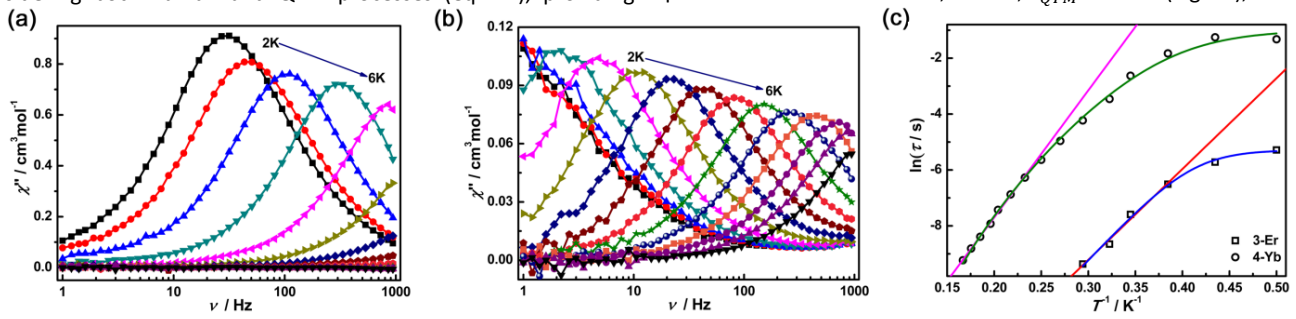

Fig. 6 Frequency dependence of out-of-phase ac susceptibility data under 1000 Oe dc field for **3** (a) and **4** (b). Temperature dependence of the relaxation times for **3** and **4** (c). The red and pink lines are the best fits to an Arrhenius law. The blue line is fit for the sum of Orbach and QTM processes. The green line is fit for Raman plus QTM processes.

$$\tau^{-1} = \tau_0^{-1}\exp(-U_{eff}/k_BT) + \tau_{QTM}^{-1} \quad (3)$$

$$\tau^{-1} = CT^n + \tau_{QTM}^{-1} \quad (4)$$

is consistent with other Yb-based SMMs. [23]

Magnetic hysteresis measurements were performed on all complexes below 3 K with a field sweep rate of 200 Oe s^{-1}. No obvious hysteresis loops were detected for complexes **1**-**4** at 2 K, which indicates fast relaxation of magnetization (Fig. S15). For **5** (the diluted sample), hysteresis loop can be observed below 2.5 K (Fig. 7), confirming that the magnetic relaxation was slowed down by dilution.

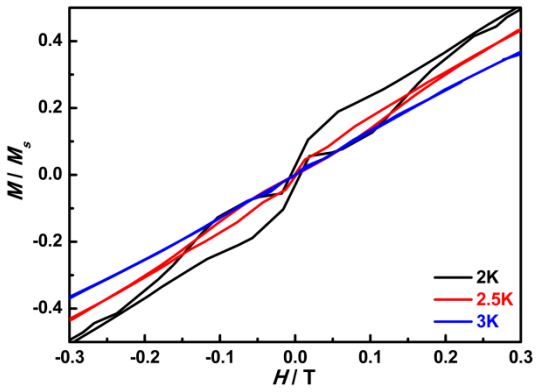

Fig. 7 Hysteresis loops for **5** normalized to the saturated magnetization measured between 2 and 3 K using a sweep rate of 200 Oe s^{-1}.

Dielectric and ferroelectric properties

Complexes **1**-**4** are isostructural and crystalline in polar space group $P2_1$, therefore, only complex **2** was selected to study their dielectric and ferroelectric properties. The value of dielectric constant is about 34 at room temperature (Fig. S16), which is comparable to those observed in other molecular ferroelectrics.[24] There is no thermal anomaly in the temperature range of 123-293 K at 1 MHz (Fig. S16), proving that no phase transitions take place below room temperature, which is consistent with the results from single crystal X-ray diffraction and DSC characterizations. To investigate the ferroelectricity of **2**, polarization measurements as function of external electric field were carried out using single crystals at various temperatures. However, no hysteresis was observed even at low temperature (Fig. S17), indicating weak spontaneous polarization of **2**.

Conclusions

A family of Ln complexes constructed from the NAS ligand has been reported. All complexes consist of a lanthanide monomer in which the lanthanide ion possesses an eight coordinated square antiprism geometry. The optical activity of these complexes was verified by CD spectra. Weak intermolecular dipolar interactions were observed in the Dy analogue, which was successfully diminished by magnetic dilution. Magnetic relaxation was detected for **2**-**4** with Kramers ions, whereas almost no ac signals was observed for **1** containing non-Kramers ion. The observation of magnetic relaxation simultaneously in Dy, Er and Yb analogues bearing the same coordination environments is rare. The energy barriers extracted from the ac data are 53, 32 and 45 K for **2**-**4**, respectively. To the best of our knowledge, these complexes represent the first examples of pure 4f sulfonate-based SMMs. This work showcase that the overlooked sulfonates is a promising group of organic ligands to synthesise Ln-based SMMs as well as more studies are required to fully understand their influence on the magnetic behaviour of target products. These studies are underway in our laboratory.

Conflicts of interest

There are no conflicts to declare

Acknowledgements

This work was supported by the National Natural Science Foundation of China (21501093) and the Natural Science Foundation of Jiangsu Province (BK20150768). BL and ZGG thanks for the financial support from NSFC of China (21401112 and 21601189).

Notes and references

1 (a) A. Caneschi, D. Gatteschi, R. Sessoli, A. L. Barra, L. C. Bruel and M. Guillot, *J. Am. Chem. Soc.*, 1991, **113**, 5873; (b) R. Sessoli, D. Gatteschi, A. Caneschi and M. A. Novak, *Nature*, 1993, **141**, 365; (c) R. Bagai and G. Christou, *Chem. Soc. Rev.*, 2009, **38**, 1011; (d) G. Christou, D. Gatteschi and D. N. Hendrickson, *MRS Bull*. 2000, **25**, 66; (e) L. Thomas, F. Lionti, R. Ballou, D. Gatteschi, R. Sessoli and B. Barbara, *Nature*, 1996, **383**, 145; (f) D. Gatteschi, R. Sessoli, *Angew. Chem. Int. Ed.*, 2003, **42**, 268.

2 (a) E. Moreno-Pineda, C. Godfrin, F. Balestro, W. Wernsdorfer and M. Ruben, *Chem. Soc. Rev.*, 2018, **47**, 501; (b) F. Troiani and M. Affronte, *Chem. Soc. Rev.*, 2011, **40**, 3119; (c) L. Bogani and W. Wernsdorfer, *Nat. Mater.*, 2008, **7**, 179; (d) M. N. Leuenberger, D. Loss, *Nature*, 2001, **414**, 789.

3 (a) R. Sessoli and A. K. Powell, *Coord. Chem. Rev.*, 2009, **253**, 2328; (b) L. Sorace, C. Benelli and D. Gatteschi, *Chem. Soc. Rev.*, 2011, **40**, 3092; (c) J. D. Rinehart and J. R. Long, *Chem. Sci.*, 2011, **2**, 2078; (d) D. N. Woodruff, R. E. P. Winpenny, R. A. Layfield, *Chem. Rev.*, 2013, **113**, 5110; (e) P. Zhang, Y. N. Guo, J. Tang, *Coord. Chem. Rev.*, 2013, **257**, 1728; (f) Y. S. Meng, S. D. Jiang, B. W. Wang and S. Gao, *Acc. Chem. Res.*, 2016, **49**, 2381.

4 (a) S. G. McAdams, A. M. Ariciu, A. K. Kostopoulos, J. P. S. Walsh and F. Tuna, *Coord. Chem. Rev.*, 2017, **346**, 216; (b) J. L. Liu, Y. C. Chen and M. L. Tong, *Chem. Soc. Rev.*, 2018, **47**, 2431; (c) S. K. Gupta and R. Murugavel, *Chem. Commun.*, 2018, **54**, 3685.

5 (a) F. S. Guo, B. M. Day, Y. C. Chen, M. L. Tong, A. Mansikkamaki and R. A. Layfield, *Angew. Chem. Int. Ed.*, 2017, **56**, 11445; (b) C. A. P. Goodwin, F. Ortu, D. Reta, N. F. Chilton and D. P. Mills, *Nature*, 2017, **548**, 439; (c) L. Ungur, J. J. Le Roy, I. Korobkov, M. Murugesu and L. F. Chibotaru, *Angew. Chem. Int. Ed.*, 2014, **53**, 4413; (d) K. R. Meihaus and J. R. Long, *J. Am. Chem. Soc.*, 2013, **135**, 17952.

6 (a) Y. C. Chen, J. L. Liu, L. Ungur, J. Liu, Q. W. Li, L. F. Wang, Z. P. Ni, F. Chibotaru, X. M. Chen and M. L. Tong, *J. Am. Chem. Soc.*, 2016, **138**, 2829; (b) S. K. Gupta, T. Rajeshkumar, G. Rajaraman and R. Murugavel, *Chem. Sci.*, 2016, **7**, 5181; (c) Y. C. Chen, J. L. Liu, W. Wernsdorfer, D. Liu, L. F. Chibotaru, X. M. Chen and M. L. Tong, *Angew. Chem. Int. Ed.*, 2017, **56**, 4996.

7 (a) Y. S. Ding, N. F. Chilton, R. E. P. Winpenny, Y. Z. Zheng, *Angew. Chem. Int. Ed.*, 2016, **55**, 16071; (b) J. Liu, Y. C. Chen, J. L. Liu, V. Vieru, L. Ungur, J. H. Jia, F. Chibotaru, Y. Lan, W. Wernsdorfer, S. Gao, X. M. Chen and M. L. Tong, *J. Am. Chem. Soc.*, 2016, **138**, 5441.

8 (a) N. Ishikawa, M. Sugita, T. Ishikawa, S. Koshihara and Y. Kaizu, *J. Am. Chem. Soc.*, 2003, **125**, 8694; (b) C. R. Ganivet, B. Ballesteros, G. de la Torre, J. M. Clemente-Juan, E. Coronado and T. Torres, *Chem. Eur. J.*, 2013, **19**, 1457.

9 (a) M. Andruh, *Dalton Trans.*, 2015, **44**, 16633; (b) S. Y. Lin, W. Wernsdorfer, L. Ungur, A. K. Powell, Y. N. Guo, J. Tang, L. Zhao, L. F. Chibotaru and H. J. Zhang, *Angew. Chem. Int. Ed.*, 2012, **51**, 12767; (c) Y. N. Guo, G. F. Xu, W. Wernsdorfer, L. Ungur, Y. Guo, J. Tang, H. J. Zhang, L. F. Chibotaru and A. K. Powell, *J. Am. Chem. Soc.*, 2011, **133**, 11948; (d) F. Habib and M. Murugesu, *Chem. Soc. Rev.*, 2013, **42**, 3278; (e) P. H. Lin, T. J. Burchell, L. Ungur, L. F. Chibotaru, W. Wernsdorfer and M. Murugesu, *Angew. Chem. Int. Ed.*, 2009, **48**, 9489; (f) K. Liu, W. Shi and P. Cheng, *Coord. Chem. Rev.*, 2015, **289-290**, 74; (g) W. B. Sun, P. F. Yan, S. D. Jiang, B. W. Wang, Y. Q. Zhang, H. F. Li, P. Chen, Z. M. Wang and S. Gao, *Chem. Sci.*, 2016, **7**, 684; (h) M. Ren, Z. L. Xu, S. S. Bao, T. T. Wang, Z. H. Zheng, R. A. Ferreira, L. M. Zheng and L. D. Carlos, *Dalton Trans.*, 2016, **45**, 2974; (i) F. Gao, X. Feng, L. Yang and X. Chen, *Dalton Trans.*, 2016, **45**, 7476.

10 (a) S. D. Jiang, B. W. Wang, G. Su, Z. M. Wang and S. Gao, *Angew. Chem. Int. Ed.*, 2010, **49**, 7448; (b) P. P. Cen, S. Zhang, X. Y. Liu, W. M. Song, Y. Q. Zhang, G. Xie and S. P. Chen, *Inorg. Chem.*, 2017, **56**, 3644; (c) H. L. Gao, S. X. Huang, X. P. Zhou, Z. Liu and J. Z. Cui, *Dalton Trans.*, 2018, **47**, 3503; (d) X. Yao, P. Yan, G. An, Y. Li, W. Li and G. Li, *Dalton Trans.*, 2018, **47**, 3976; (e) N. F. Chilton, S. K. Langley, B. Moubaraki, A. Soncini, S. R. Batten and K. S. Murray, *Chem. Sci.*, 2013, **4**, 1719; (f) X. L. Mei, Y. Ma, L. C. Li and D. Z. Liao, *Dalton. Trans*, 2012, **41**, 505; (g) G. J. Chen, Y. N. Guo, J. L. Tian, J. Tang, W. Gu, X. Liu, S. P. Yan, P. Cheng and D. Z. Liao, *Chem. Eur. J.*, 2012, **18**, 2484.

11 (a) S. Sakaue, A. Fuyuhiro, T. Fukuda and N. Ishikawa, *Chem. Commun.*, 2012, **48**, 5337; (b) K. Katoh, S. Yamashita, N. Yasuda, Y. Kitagawa, B. K. Breedlove, Y. Nakazawa and M. Yamashita, *Angew. Chem. Int. Ed.*, 2018, **57**, 9262; (c) T. Morita, M. Damjanovic, K. Katoh, Y. Kitagawa, N. Yasuda, Y. Lan, W. Wernsdorfer, B. K. Breedlove, M. Enders and M. Yamashita, *J. Am. Chem. Soc.*, 2018, **140**, 2995; (d) H. Wang, B. W. Wang, Y. Bian, S. Gao and J. Jiang, *Coord. Chem. Rev.*, 2016, **306**, 195; (e) Y. Chen, F. Ma, X. Chen, B. Dong, K. Wang, S. Jiang, C. Wang, X. Chen, D. Qi, H. Sun, B. Wang, S. Gao and J. Jiang, *Inorg. Chem.*, 2017, **56**, 13889.

12 (a) A. V. Gavrikov, N. N. Efimov, Z. V. Dobrokhotova, A. B. Ilyukhin, P. N. Vasilyev and V. M. Novotortsev, *Dalton Trans.*, 2017, **46**, 11806; (b) R. P. Li, Q. Y. Liu, Y. L. Wang, C. M. Liu and S. J. Liu, *Inorg. Chem. Front.*, 2017, **4**, 1149; (c) G. J. Zhou, Y. S. Ding and Y. Z. Zheng, *Dalton Trans.*, 2017, **46**, 3100; (d) E. C. Mazarakioti, J. Regier, L. Cunha-Silva, W. Wernsdorfer, M. Pilkington, J. Tang and T. C. Stamatatos, *Inorg. Chem.*, 2017, **56**, 3568; (e) Y. B. Lu, X. M. Jiang, S. D. Zhu, Z. Y. Du, C. M. Liu, Y. R. Xie and L. X. Liu, *Inorg. Chem.*, 2016, **55**, 3738; (f) E. Bartolome, J. Bartolome, S. Melnic, D. Prodius, S. Shova, A. Arauzo, J. Luzon, F. Luis and C. Turta, *Dalton Trans.*, 2013, **42**, 10153; (g) S. J. Liu, J. P. Zhao, W. C. Song, S. D. Han, Z. Y. Liu and X. H. Bu, *Inorg. Chem.*, 2013, **52**, 2103; (h) L. Liang, G. Peng, G. Li, Y. Lan, A. K. Powell and H. Deng, *Dalton Trans.*, 2012, **41**, 5816; (i) B. Joarder, A. K. Chaudhari, G. Rogez and S. K. Ghosh, *Dalton Trans.*, 2012, **41**, 7695.

13 (a) K. H. Zangana, E. Moreno Pineda and R. E. Winpenny, *Dalton Trans.*, 2015, **44**, 12522; (b) D. Zeng, M. Ren, S. S. Bao, J. S. Feng, L. Li and L. M. Zheng, *Chem. Commun.*, 2015, **51**, 2649; (c) M. Ren, S. S. Bao, N. Hoshino, T. Akutagawa, B. Wang, Y. C. Ding, S. Wei and L. M. Zheng, *Chem. Eur. J.*, 2013, **19**, 9619; (d) S. K. Langley, K. R. Vignesh, K. Holton, S. Benjamin, G. B. Hix, W. Phonsri, B. Moubaraki, K. S. Murray and G. Rajaraman, *Inorganics*, 2018, **6**, 61.

14 (a) R. J. Blagg, C. A. Muryn, E. J. McInnes, F. Tuna and R. E. Winpenny, *Angew. Chem. Int. Ed.*, 2011, **50**, 6530; (b) R. J. Blagg, F. Tuna, E. J. McInnes and R. E. Winpenny, *Chem. Commun.*, 2011, **47**, 10587; (c) R. J. Blagg, L. Ungur, F. Tuna, J. Speak, P. Comar, D. Collison, W. Wernsdorfer, E. J. McInnes, L. F. Chibotaru and R. E. Winpenny, *Nat. Chem.*, 2013, **5**, 673; (d) J. Xiong, H. Y. Ding, Y. S. Meng, C. Gao, X. J. Zhang, Z. S. Meng, Y. Q. Zhang, W. Shi, B. W. Wang and S. Gao, *Chem. Sci.*, 2017, **8**, 1288.

15 (a) S. D. Jiang, B. W. Wang, H. L. Sun, Z. M. Wang and S. Gao, *J. Am. Chem. Soc.*, 2011, **133**, 4730; (b) K. R. Meihaus and J. R. Long, *J. Am. Chem. Soc.*, 2013, **135**, 17952; (c) R. A.

Layfield, *Organometallics*, 2014, **33**, 1084; (d) T. Pugh, N. F, Chilton and R. A. Layfield, *Angew. Chem. Int. Ed.*, 2016, **55**, 11082; (e) J. J. Le Roy, L. Ungur, I. Korobkov, L. F. Chibotaru and M. Murugesu, *J. Am. Chem. Soc.*, 2014, **136**, 8003; (f) K. L. Harriman and M. Murugesu, *Acc. Chem. Res.*, 2016, **49**, 1158.

16 (a) J. W. Sharples and D. Collison, *Coord. Chem. Rev.*, 2014, **260**, 1; (b) G. Abbas, Y. Lan, G. E. Kostakis, W. Wernsdorfer, C. E. Anson and A. K. Powell, *Inorg. Chem.*, 2010, **49**, 8067; (c) G. Abbas, Y. Lan, V. Mereacre, W. Wernsdorfer, R. Clerac, G. Buth, M. T. Sougrati, F. Grandjean, G. J. Long, C. E. Anson and A. K. Powell, *Inorg. Chem.*, 2009, **48**, 9345; (d) S. K. Langley, L. Ungur, N. F. Chilton, B. Moubaraki, L. F. Chibotaru and K. S. Murray, *Inorg. Chem.*, 2014, **53**, 4303; (e) S. K. Langley, D. P. Wielechowski, V. Vieru, N. F. Chilton, B. Moubaraki, B. F. Abrahams, L. F. Chibotaru, and K. S. Murray, *Angew. Chem. Int. Ed.*, 2013, **52**, 12014.

17 (a) Y. Ohki, Y. Suzuki, T. Takeuchi and A. Ouchi, *Bull. Chem. Soc. Jpn.*, 1988, **61**, 393; (b) Y. Ohki, Y. Suzuki, M. Nakamura, M. Shimoi and A. Ouchi, *Bull. Chem. Soc. Jpn.*, 1985, **58**, 2968; (c) F. Gándara, A. García-Cortés, C. Cascales, B. Gómez-Lor, E. Gutiérrez-Puebla, M. Iglesias, A. Monge and N. Snejko, *Inorg. Chem.*, 2007, **46**, 3475; (d) F. Gándara, E. G. Puebla, M. Iglesias, D. M. Proserpio, N. Snejko and M. Á. Monge, *Chem. Mater.*, 2009, **21**, 655; (e) J. Perles, N. Snejko, M. Iglesias and M. Á. Monge, *J. Mater. Chem.*, 2009, **19**, 6504; (f) X. Yang, J. H. Rivers, W. J. McCarty, M. Wiester and R. A. Jones, *New J. Chem.*, 2008, **32**, 790; (g) H. Li, T. Sheng, Z. Xue, X. Zhu, S. Hu, Y. Wen, R. Fu, C. Zhuo and X. Wu, *CrystEngComm*, 2017, **19**, 2106; (h) A. García-García, I. Oyarzabal, J. Cepeda, J. M. Seco, A. A. García-Valdivia, S. Gómez-Ruiz, A. Salinas-Castillo, D. Choquesillo-Lazarte and A. Rodríguez-Diéguez, *New J. Chem.*, 2018, **42**, 832.

18 (a) N. E. Chakov, W. Wernsdorfer, K. A. Abboud, D. N. Hendrickson and G. Christou, *Dalton Trans.*, 2003, 2243; (b) S. K. Langley, B. Moubaraki and K. S. Murray, *Aust. J. Chem.*, 2014, **67**, 1601.

19 G. M. Sheldrick, *Acta Cryst. C*, 2015, **71**, 3.

20 (a) M. Pinsky and D. Avnir, *Inorg. Chem.*, 1998, **37**, 5575; (b) D. Casanova, J. Cirera, M. Llunell, P. Alemany, D. Avnir and S. Alvarez, *J. Am. Chem. Soc.*, 2004, **126**, 1755; (c) J. Cirera, E. Ruiz and S. Alvarez, *Chem. Eur. J.,* 2006, **12**, 3162.

21 Y. N. Guo, G. F. Xu, Y. Guo and J. Tang, *Dalton Trans.*, 2011, **40**, 9953.

22 (a) A. Singh and K. N. Shrivastava, *Phys. Status Solidi B*, 1979, **95**, 273; (b) K. N. Shrivastava, *Phys. Status Solidi B*, 1983, **117**, 437.

23 (a) J. L. Liu, K. Yuan, J. D. Leng, L. Ungur, W. Wernsdorfer, F. S. Guo, L. F. Chibotaru and M. L. Tong, *Inorg. Chem.*, 2012, **51**, 8538; (b) F. Pointillart, O. Cador, B. Le Guennic and L. Ouahab, *Coord. Chem. Rev.*, 2017, **346**, 150; (c) I. Oyarzabal, B. Artetxe, A. Rodriguez-Dieguez, J. Garcia, J. M. Seco and E. Colacio, *Dalton Trans.*, 2016, **45**, 9712.

24 (a) T. Hang, W. Zhang, H. Y. Ye and R. G. Xiong, *Chem. Soc. Rev.*, 2011, **40**, 3577; (b) Z. Chen, Y. Shen, L. Li, H. Zou, X. Fu, Z. Liu, K. Wang and F. Liang, *Dalton Trans.*, 2017, **46**, 15032.